IEEE Access
Multidisciplinary | Rapid Review | Open Access Journal

Received February 7, 2021, accepted February 16, 2021, date of publication February 19, 2021, date of current version March 2, 2021.

Digital Object Identifier 10.1109/ACCESS.2021.3060388

Improvement of the Constant-Power Speed Range of Surface-Permanent Magnet Machine Using Winding Switching

STANISLAV SIN, ALI ROSHANZAMIR, AND BYUNG-IL KWON, (Senior Member, IEEE)
Department of Electrical and Electronic Engineering, Hanyang University, Ansan 15588, South Korea

Corresponding author: Byung-Il Kwon (bikwon@hanyang.ac.kr)

This work was supported in part by the National Research Foundation of Korea Grant funded by the Korean Government (Ministry of Science) under Grant NRF-2020R1A2B5B01002400, and in part by the BK21FOUR Program through the National Research Foundation of Korea within the Ministry of Education.

ABSTRACT In this study, a cumulative/differential winding switching method is proposed for the extended constant power operation (CPO) of a surface-permanent magnet (SPM) machine. In this method, the three-phase winding of the machine is divided into two equal sub-phase sets, and field weakening is realized by switching the interconnections between the sets. The field-weakening ratio depends on the shift angle between the two sub-phase sets. Hence, it is possible to adjust this angle to obtain a constant power speed range (CPSR). The dependence of the CPO possibility of the proposed winding switching method on the shift angle is analyzed. The analytical requirement for the CPO is formulated, and an algorithm for choosing an optimal winding layout is proposed. The winding switching method is then implemented on a four-pole 24-slotted surface-permanent magnet synchronous machine, and the stator winding is changed according to the CPO requirement. The finite element modeling and experimental results verify the extension of the CPSR to four per unit (pu), using the proposed winding switching method with a suitable shift angle. Hence, this method is suitable for constant-power applications, such as traction and electric vehicles.

INDEX TERMS Field-weakening, constant power speed range, permanent magnet machines, winding reconfiguration, winding switching.

I. INTRODUCTION

Modern hard magnetic materials have a high residual flux and coercive force. Typically, for the same output torque, the dimensions of permanent magnet synchronous machines (PMSMs) are smaller than those of traditional wound field synchronous machines (WFSMs). The absence of field winding also decreases copper losses, improving the energy efficiency. However, the drawback of magnet excitation, compared to field winding excitation, is the complicated field-weakening operation.

The rotating electromagnetic field created by the rotor induces the back EMF in the stator winding. When the rotation speed increases, a higher supply voltage is required to oppose this back EMF. Apparently, the supply voltage is limited. The maximal speed, which can be achieved at a given voltage limit is referred to as the rated speed. In a conventional WFSM, the speed can be increased by decreasing the field current; this regime is referred to as field weakening. However, in the case of a PMSM, it is impossible to directly control the field flux. This complicates its operation above the rated speed. It is necessary to oppose the magnet flux by applying a negative d-axis current (demagnetizing current). It can be said that this current creates a negative flux. The value of this flux depends on the synchronous inductance [1]–[5]

$$\lambda_{fw} = L_d I_m \tag{1}$$

where λ_{fw} is the negative flux created by the demagnetizing current, L_d is the synchronous inductance, and I_m is the rated machine current.

Surface-permanent magnet (SPM) machines typically have lower L_d compared to interior-permanent magnet machines because of their high magnetic reluctance along the d-axis. This causes a worse constant-power capability in the flux-weakening regime [6]. However, owing to their simple structure and low cost, it is still desirable to implement SPM machines in a constant-power application, where the output torque is inversely proportional to the speed. Such applications include traction and electric vehicles.

The associate editor coordinating the review of this manuscript and approving it for publication was Qinfen Lu.

Various methods have been proposed for extending the constant power speed range (CPSR) of SPM machines. For example, an external inductor with a stator winding was connected to improve the CPSR of an SPM machine; however, it introduced additional copper losses and increased the inverter volt-ampere rating [7]. The next method involved the use of a voltage boost converter to increase the available voltage; however, this converter often required a large inductor, which resulted in a large drive cost and bulkiness [8], [9]. The winding switching methods changed the winding configuration using external switches to decrease the effective back EMF [10]–[23].

Among the above-mentioned methods, winding switching is relatively simple, low-cost, and flexible. However, it often requires machine rewinding, which increases the cost. The need for additional switches, gating circuits, and a more complicated control board also increases drive cost. Another disadvantage of this type of method is the switching transient, which can damage a machine or inverter. Several studies have addressed this problem and demonstrated the possibility of winding switching during machine operation [14]–[16]. In the past few years, cumulative/differential winding switching for a three-phase double inverter has been reported in existing literature [17]–[21]. In this winding switching method, each phase was divided into two equal open-ended sub-phases, and the winding configuration was changed so that each sub-phase pair either added or subtracted their flux linkages. The flux linkage was decreased up to 3.73 times for a four-pole machine, and in [18], the possibility of the constant-power operation of a two-pole machine using this winding switching was proved. In [22] and [23], the cumulative/differential winding switching was implemented on a three-phase single inverter, and the transistor number was decreased; however, the constant power operation (CPO) was not achieved. Therefore, this method could be implemented only in discrete-type drives.

In this work, cumulative/differential winding switching is proposed to extend the CPSR of the SPM machine to approximately 4 pu. It is demonstrated that the field-weakening ratio of the cumulative/differential winding switching method can be adjusted by shifting the angle between the sub-phase sets. The theoretical principles underlying this winding switching method are formulated, and the requirements for the CPO are determined. A suitable shift angle is chosen based on the CPO requirement. The FEA and experimental results verify the improvement of the CPSR using the proposed winding switching method with a suitable shift angle.

II. PROPOSED WINDING SWITCHING METHOD

The winding switching method is proposed for the four-pole, 24-slot, three-phase SPM machine, with distributed winding and sinusoidal back EMF. The machine cross-section and simplified diagram are shown in Fig. 1(a) and (b), respectively. As mentioned before, the three-phase winding of the SPM machine is divided into six equal sub-phases: A, B, C, X, Y, and Z. The ABC and XYZ sub-phases are shifted by ϕ electrical degrees.

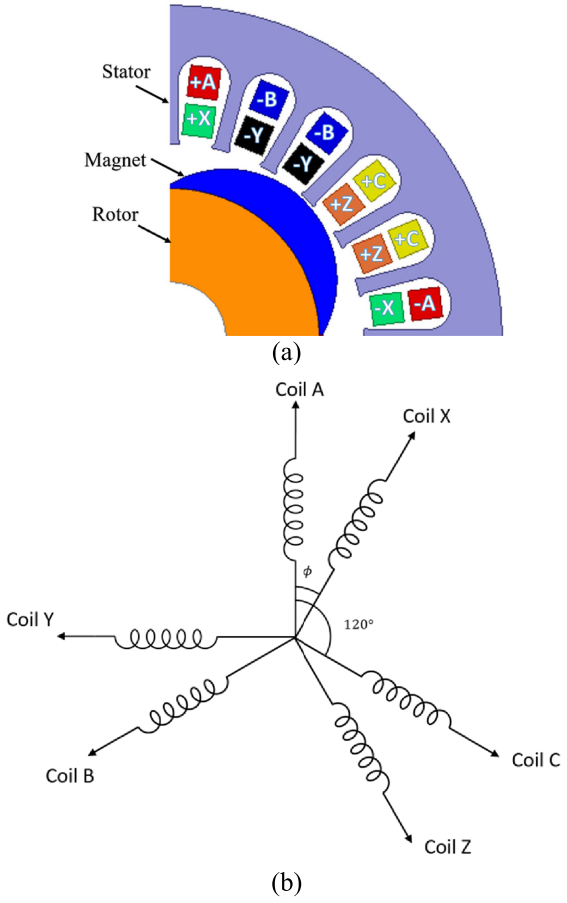

FIGURE 1. (a) Machine cross section; (b) simplified machine diagram.

The switch arrangement is similar to the one in [23] and is shown in Fig. 2(a). There are four operable modes; the switch states for each mode are listed in Table 1 for convenience.

Mode I is a basic three-phase wye-connected SPM machine. Switches S1–S3 and S7–S9 are ON, whereas S4–S6 and S10–S12 are OFF, as shown in Fig. 2(b). The sub-phase pairs A and X; B and Y; and C and Z form phases U, V, and W, respectively. If sub-phase A is chosen as a reference, the fundamental component of the line-to-line flux linkage can be calculated as follows:

$$\begin{aligned}\lambda_{l1} &= (\lambda_A + \lambda_X - \lambda_B - \lambda_Y) \\ &= \lambda sin\,(\omega t) + \lambda sin\,(\omega t + \phi) - \lambda sin\left(\omega t + \frac{2\pi}{3}\right) \\ &\quad - \lambda sin\left(\omega t + \frac{2\pi}{3} + \phi\right) \end{aligned} \tag{2}$$

where λ_{l1} is the line flux linkage in mode I, λ_A, λ_X, λ_B, and λ_Y are the flux linkages of the corresponding sub-phases, λ is the flux linkage of one sub-phase, ϕ is the electrical angle between the ABC and XYZ sub-phases, and ω is the electrical angular frequency.

Mode II is shown in Fig. 2(c), switches S1–S3 and S10–S12 are ON, whereas the remaining switches are OFF.

TABLE 1. Operation modes of the machine.

Mode	ON	OFF
Mode I	S1, S2, S3, S7, S8, S9	S4, S5, S6, S10, S11, S12
Mode II	S1, S2, S3, S10, S11, S12	S4, S5, S6, S7, S8, S9
Mode III	S4, S5, S6, S7, S8, S9	S1, S2, S3, S10, S11, S12
Mode IV	S4, S5, S6, S10, S11, S12	S1, S2, S3, S7, S8, S9

As can be observed, the sub-phase pairs are similar; however, the three phases form a delta connection. Hence, the line flux linkage is equal to the phase flux linkage.

$$\begin{aligned}\lambda_{l2} &= -(\lambda_B + \lambda_Y) \\ &= -\left[\lambda sin\left(\omega t + \frac{2\pi}{3}\right) - \lambda sin\left(\omega t + \frac{2\pi}{3} + \phi\right)\right]\end{aligned} \tag{3}$$

Mode III is shown in Fig. 2(d). The ON switches are S4–S6 and S7–S9, whereas the OFF switches are S1–S3 and S10–S12. The sub-phase pairs A and Z, B and X, and C and Y correspond to the wye-connected phases U, V, and W, respectively. The line flux linkage in this mode is:

$$\begin{aligned}\lambda_{l3} &= (\lambda_A + \lambda_Z - \lambda_B - \lambda_X) \\ &= \lambda sin\,(\omega t) + \lambda sin\left(\omega t + \frac{4\pi}{3} + \phi\right) \\ &\quad - \lambda sin\left(\omega t + \frac{2\pi}{3}\right) - \lambda sin(\omega t + \phi)\end{aligned} \tag{4}$$

Mode IV is shown in Fig. 2(e). Switches S4–S6 and S10–S12 are ON, whereas S1–S3 and S7–S9 are OFF, which results in the delta-connected sub-phase pairs A and Z, B and X, and C and Y. The line flux linkage is expressed as follows:

$$\lambda_{l4} = (\lambda_A + \lambda_Z) = \lambda sin\,(\omega t) + \lambda sin\left(\omega t + \frac{4\pi}{3} + \phi\right) \tag{5}$$

From equations (2)–(5), the field-weakening ratio can be calculated as follows:

$$K_2 = \frac{\lambda_{l1}}{\lambda_{l2}} = \sqrt{3} \tag{6}$$

$$K_3 = \lambda_{l1}/\lambda_{l3} \tag{7}$$

$$K_4 = \frac{\lambda_{l1}}{\lambda_{l4}} = K_3\sqrt{3} \tag{8}$$

where K is the field-weakening ratio and the subscript number denotes the operation mode. It is well known that line parameters are $\sqrt{3}$ times higher than their phase counterparts. Because the winding is changed from Y to Δ in the transitions from mode I to mode II and from mode III to mode IV, the K_2 and K_4 relations have a $\sqrt{3}$ multiplier. However, the K_3 depends on the angle ϕ. For the given slotted machine, which can be discretely adjusted with a 30° step. The field-weakening ratios for certain ϕ values are listed in Table 2. As can be observed, the 60° shift is pointless because the flux linkage is 0 Wb. Hence, $\phi = 0°$ and $\phi = 30°$ winding layouts are considered for the extended CPSR.

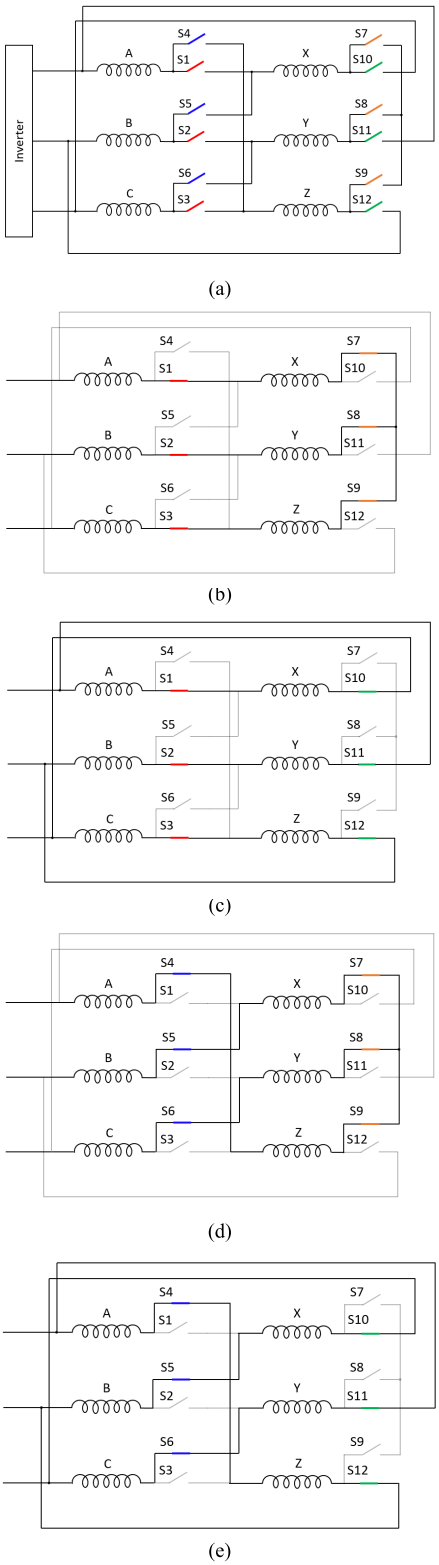

FIGURE 2. (a) Proposed winding switching method. (b) Mode I, (c) mode II, (d) mode III, (e) mode IV.

TABLE 2. Effect of changing shift between ABC and XYZ.

	$\phi = 0°$	$\phi = 30°$	$\phi = 60°$
K_2	1.732	1.732	1.732
K_3	2	3.732	∞
K_4	3.346	6.464	∞

III. CONSTANT POWER CAPABILITY ANALYSIS

The analytical requirements for CPO are presented in this section. The analysis is based on the analytical model from [23], which is shown below.

A. ANALYTICAL MODEL OF THE WINDING SWITCHING METHOD

The decrease in the flux linkage because of winding switching is shown in (2)–(8). Because the back EMF is proportional to the electrical angular frequency, it can be inferred that the speed range of the machine was increased. However, for a constant power capability analysis, it is necessary to analyze the voltage and torque equations for each mode.

In modes I and II, the voltage equation for phase U is expressed as follows:

$$\begin{aligned} V_{U1} = {} & I_U R + (L_{aa} + L_{xx} + 2 * L_{ax}) \frac{dI_U}{dt} \\ & + \left(L_{ab} + L_{xb} + L_{ay} + L_{xy}\right) \frac{dI_V}{dt} \\ & + (L_{ac} + L_{xc} + L_{az} + L_{xz}) \frac{dI_W}{dt} + \omega\lambda cos(\omega t) \\ & + \omega\lambda cos(\omega t + \phi) \end{aligned} \tag{9}$$

where V is the phase voltage, the subscript denotes the phase name, I is the phase current, R is the phase resistance, L_{aa} and L_{ax} are the self-inductance of one sub-phase and mutual inductance between the corresponding sub-phases, and ω is the electrical angular frequency.

The mutual inductance for the sinewave machine can be calculated as follows.

$$L_{ax} = L_m cos(\alpha) \tag{10}$$

where α is the electrical angle between the sub-phases A and X.

The torque in modes I and II is given by

$$T_{12} = \frac{3}{2}\frac{P}{2} \cdot \lambda_{l2} I_q \tag{11}$$

where T is the electromagnetic torque, P is the number of poles, and I_q is the q-axis phase current. It should be noted that in (11), the line flux linkage λ_{l2} is equal to the phase flux linkage in modes I and II.

The phase and line parameters of the wye connection are related as follows:

$$V_l = V_{ph}\sqrt{3} \tag{12}$$
$$I_l = I_{ph} \tag{13}$$
$$R_l = 2R_{ph} \tag{14}$$
$$L_l = 2L_{ph} \tag{15}$$

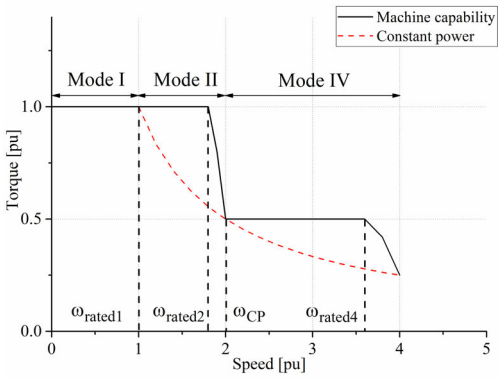

FIGURE 3. Analytically predicted torque-speed curve.

where subscripts l and ph represent the line and phase parameters, respectively.

For the delta connection, these parameters relate as follows:

$$V_l = V_{ph} \tag{16}$$
$$I_l = I_{ph}\sqrt{3} \tag{17}$$
$$R_l \frac{2}{3} R_{ph} \tag{18}$$
$$L_l = \frac{2}{3} L_{ph} \tag{19}$$

In modes III and IV, the phase voltages are:

$$\begin{aligned} V_{U3} = {} & (L_{aa} + L_{zz} + 2 * L_{az}) \frac{dI_U}{dt} + (L_{ab} + L_{zb} + L_{ax} + L_{zx}) \\ & \times \frac{dI_V}{dt} + \left(L_{ac} + L_{zc} + L_{ay} + L_{zy}\right) \frac{dI_W}{dt} \\ & + \omega\lambda \cos(\omega t) + \omega\lambda \cos\left(\omega t + \frac{4\pi}{3} + \phi\right) \end{aligned} \tag{20}$$

Consequently, the torque in these modes is:

$$T_{34} = \frac{3}{2}\frac{P}{2} \cdot \lambda_{l4} I_q \tag{21}$$

Here, the line flux linkage λ_{l4} equals the phase linkage in modes III and IV.

B. CONSTANT POWER CAPABILITY REQUIREMENT

The torque-speed curve predicted from the above conclusions is shown in Fig. 3. The solid line represents the machine speed-torque capability curve, and the dashed line represents the torque required for the CPO. ω_{rated1}, ω_{rated2}, and ω_{rated4} are the rated speeds in modes I, II, and IV, respectively. ω_{CP} represents the minimum speed at which the rated power should be maintained to achieve continuous CPO. From (11), (13), and (17), the line current should be $\sqrt{3}$ times greater than the line current in mode I to maintain the same rated torque in mode II. Therefore, the output power exceeds one per-unit (pu) and the I_q current should be decreased. Because the back EMF is a significant part of the voltage drop, the rated speed in mode II ω_{rated2} is approximately K_2 times larger than ω_{rated1}. After ω_{rated2} the machine requires the injection of the $-I_d$ current to rotate.

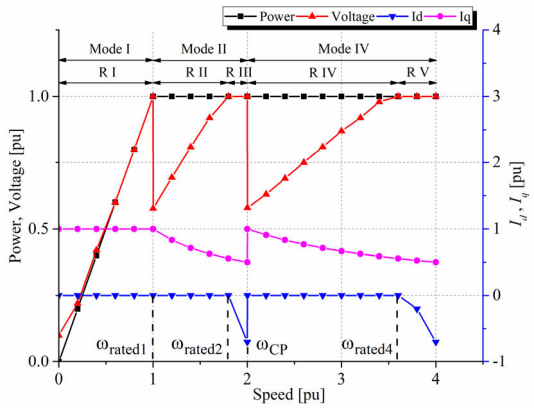

FIGURE 4. Power, voltage, and current versus speed in CPO.

Because modes III–IV have equal torque constants of $1.5 \cdot P\lambda_{l4}$, it is reasonable to skip mode III, and move from mode II to mode IV. Skipping mode III is also advantageous in terms of switching transients: 12 switches should be switched to move from mode II to mode III; however when switching from mode II to mode IV, only six switches change their state.

First, the machine in mode IV runs at $I_d = 0$ until the voltage limit is reached. The injection of $-I_d$ is required.

The machine constant power control in the proposed winding switching method is shown in Fig. 4, where the voltage, power, and dq currents per unit are shown. There are five operational regions. R I is referred to as the current-limited region; it coincides with the operation in mode I. The torque and I_q are maintained at their rated values in this region, and the machine power and voltage gradually increase to one pu.

R II is referred to as the power-limited operation region; it starts above one pu speed after winding switching is performed. In this region, the back EMF is reduced, thus, the inverter can output the rated current. However, the power reaches its rated value. To operate within the power limit, I_q should decrease at speeds from ω_{rated1} to ω_{rated2}. The output power is:

$$P_{out} = T\omega_m \tag{22}$$

where P_{out} is the output power and ω_m is the mechanical angular frequency, which is related to the electrical frequency as follows:

$$\omega_e = (\omega_m \cdot P)/2 \tag{23}$$

Considering the four-pole machine, from (11) and (23), it is clear that in mode II, the required I_q is

$$I_q = \frac{P_{out}}{1.5 \cdot \lambda_{l2}\omega_e} \tag{24}$$

which simply indicates that I_q is inversely proportional to the rotational speed.

Because the line back EMF is decreased, the machine runs at $I_d = 0$, and as shown (24), at a decreased I_q. This reduces the copper losses, thereby improving the efficiency.

In R III, starting from the speed ω_{rated2}, the voltage is once again one pu, and -I_d is injected into the winding to run further. This region is referred to as the power-, current-, and voltage-limited operation region. In this region, the rated power can be achieved at a certain speed ω_{CP}. As can be observed from (11), (21), and (6)–(8), the torque in mode IV decreases $\lambda_{l2}/\lambda_{l4} = K_3$. From (22), the CPO requirement can be formulated as follows:

$$K_3 \leq \frac{\omega_{CP}}{\omega_{rated1}} \tag{25}$$

To clarify the CPO capability, it is necessary to calculate ω_{CP} for a given machine. It is convenient to use the machine model in the *dq0* reference frame for this purpose. The required -I_d current at a given speed can be determined from the *dq0* voltage equations. The voltages in the *dq0* reference frame are:

$$V_d = RI_d - \omega_e L_q I_q \tag{26}$$

$$V_q = RI_q + \omega_e \lambda_{l2} + \omega_e L_d I_d \tag{27}$$

$$V_{ph} = \sqrt{V_d^2 + V_q^2} \tag{28}$$

where V_d and V_q are the dq-components of the phase voltage V_{ph}.

The voltage on the resistances in (26) and (27) is small compared to other components, thus, it can be neglected for simplicity. Substituting it into (28), we obtain:

$$\frac{V_{ph}^2}{\omega_e^2} = L_q^2 I_q^2 + \lambda_{l2}^2 + 2\lambda_{l2} L_d I_d + L_d^2 I_d^2 \tag{29}$$

Note that I_q in Eq. (29) is given by (24). However, the I_{dq} currents must satisfy the following limitations:

$$I_{ph} = \sqrt{I_d^2 + I_q^2} \tag{30}$$

(29) can be rewritten using Eqs. (24) and (30):

$$\begin{aligned} \frac{V_{ph}^2}{\omega_e^2} &= L_q^2 \left(\frac{P_{out}}{1.5 \cdot \lambda_{l2}\omega_e}\right)^2 + \lambda_{l2}^2 + 2\lambda_{l2} L_d \\ &\times \left[-\sqrt{I_{ph}^2 - \left(\frac{P_{out}}{1.5 \cdot \lambda_{l2}\omega_e}\right)^2}\right] \\ &+ L_d^2 \left[I_{ph}^2 - \left(\frac{P_{out}}{1.5 \cdot \lambda_{l2}\omega_e}\right)^2\right]^2 \end{aligned} \tag{31}$$

Numerically solving (31), the speed ω_{CP} at which the rated power is attainable in mode II can be obtained.

After the speed ω_{CP}, the winding is switched to mode IV, and the machine enters the R-IV region. This is analogous to region II. It should be noted that equation (24) can be used for R IV; however, the term λ_{l4} should be used instead of λ_{l2}. It is clear that the operation in R IV begins at I_q = one pu and I_d= 0, as shown in Fig. 4. It then decreases in proportion to $1/P_{out}$.

When the voltage increases to one pu, the machine enters operation R V. This is analogous to R III. By repeating the derivation process for (30) and (31) considering the decreased

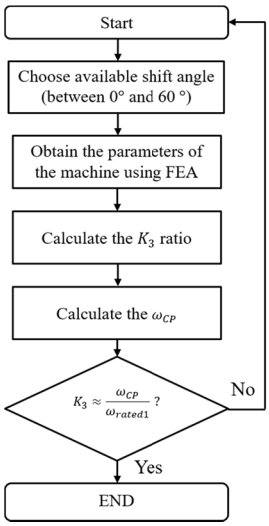

FIGURE 5. Algorithm of optimal winding layout choice.

flux linkage term λ_{l4}, the required $-I_d$ current and maximal constant-power speed can be calculated.

C. OPTIMAL WINDING LAYOUT FOR THE CONSTANT POWER OPERATION

In the previous subsection, the CPO requirement was formulated, making it possible to choose an appropriate winding layout for a given machine. The algorithm used for this process is shown in Fig. 5. In the beginning, it is necessary to choose the available values of the angle ϕ. An FEM model of the machine is then created using the chosen ϕ to obtain the machine parameters, such as the flux linkage λ of each subphase, synchronous inductance L_d, rated voltage, and rated torque. Subsequently, we calculate the field-weakening ratio K_3 from (7) using the obtained flux linkages. We then solve (31) numerically to calculate ω_{CP}, as described previously. Finally, K_3 and $\omega_{CP}/\omega_{rated1}$ are compared.

To maximize the CPSR, the right-hand and left-hand sides of (25) should be as close to each other as possible. If K_3 is smaller than $\omega_{CP}/\omega_{rated1}$, the full CPO capability of the machine is not realized.

IV. FINITE ELEMENT ANALYSIS

In this study, the proposed winding changeover method was implemented on a four-pole 24-slotted SPM machine, as shown in Fig. 1(a). A CAD model was created, for two-dimensional finite-element modeling in an "AnSys Maxwel" software. A fine sliding mesh was used to ensure the accuracy of the simulation results. The number of elements was 42832, and the minimal mean element area was $7 \times 10^{-7} mm^2$. The vector potential boundary is set to zero at the stator outer surface.

As mentioned previously, for our machine, there are two values of ϕ: 0° and 30°. Steady-state simulations were performed at a rated speed of 300 rpm for the two winding layouts. The extracted machine parameters were used to calculate ω_{CP}, and the simulation results are listed in Table 3. As can be observed from this table, the ratio $\omega_{CP}/\omega_{rated1}$ is

TABLE 3. Parameters of the machine and corresponding ω_{CP} with two winding layouts.

	$\phi = 0°$	$\phi = 30°$
Number of poles	4	
Number of slots	24	
Phase resistance	2 Ohm	
Synchronous inductance	11.360 mH	10.470 mH
Phase flux linkage	0.349 Wbrms	0.337 Wbrms
Rated speed	300 rpm	300 rpm
Rated phase current	2.5 Arms	
Rated line voltage	46.573 Vrms	43.610 Vrms
Rated torque	5.3438 Nm	5.170 Nm
ω_{CP}	645 rpm	618 rpm
K_3	2.000	3.732

2.15 for $\phi = 0°$ and 2.06 for $\phi = 30°$; hence, the winding layout with a shift angle $\phi = 0°$ is the only layout suitable for the CPO. Moreover, because this ratio is close to optimum, the machine power capability is almost fully utilized. It is worth mentioning that if the number of slots is increased, additional freedom in the ϕ choice will be achieved. It also seems beneficial to implement the proposed winding switching method on slotless machines.

In this section, the FEA results for $\phi = 0°$ are presented to verify the CPO of the given SPM machine. To confirm equations (6)–(8), the machine was simulated at a rated speed of 300 rpm without electrical loading. The line flux linkages in modes I–IV were measured and are shown in Figs. 6(a)–(d). The RMS values were 0.6039 Wb, 0.3489 Wb, 0.3020 Wb, and 0.1747 Wb in modes I – IV, respectively. This agrees well with the flux weakening ratios predicted in (6)–(8).

The decrease in flux leads to a decrease in the back EMFs and torques. The line back EMFs are shown in Figs. 7(a)–(d). As can be observed, it was 37.9453 V_{rms}, 22.0056 V_{rms}, 18.9740 V_{rms}, and 11.1495 V_{rms} in modes I–IV, respectively.

The loaded simulations were performed to obtain the torque-speed curves in modes I–IV. To maintain the rated phase current in modes II and IV, we increased the line current $\sqrt{3}$ times compared to mode I. The torque-speed curves for each mode are shown in Fig. 8, where the dashed line represents the ideal constant power curve. The rated torque values were 5.3438 Nm, 5.1676 Nm, 2.7375 Nm, and 2.5590 Nm in modes I, II, III, and IV, respectively. Consequently, the rated output power was 167.88 W. From this figure, it is clear that CPO was possible for the given machine.

The torque in the delta connections was 3.41% lower than that in the wye connections. This is because of the triple harmonic current, which circulates in the delta winding

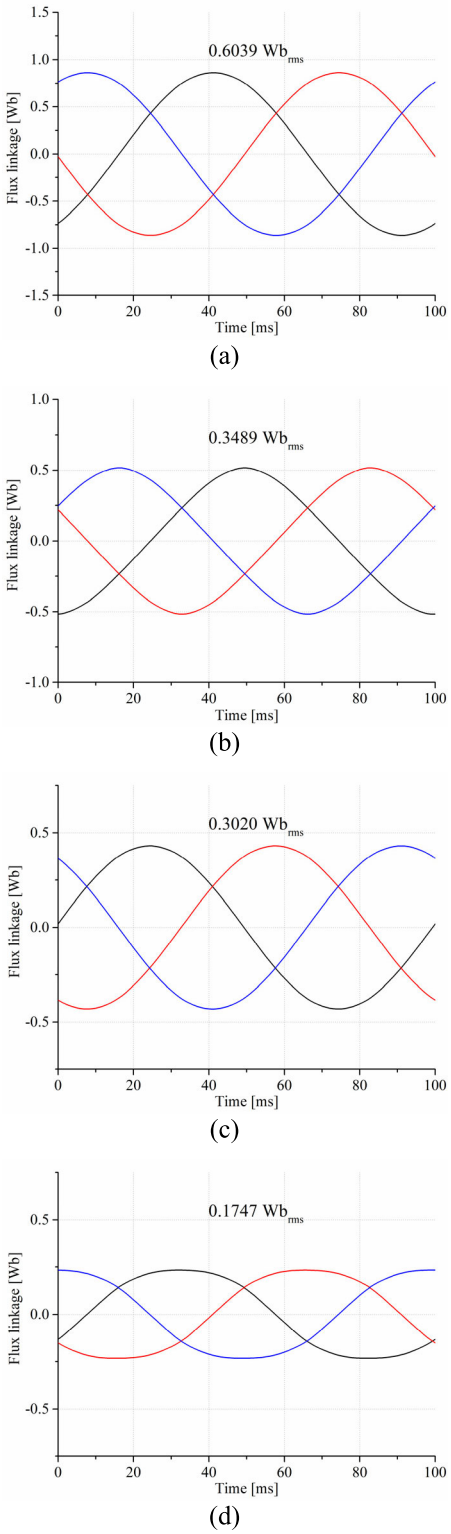

FIGURE 6. Simulated line flux linkages in (a) mode I; (b) mode II; (c) mode III; (d) mode IV.

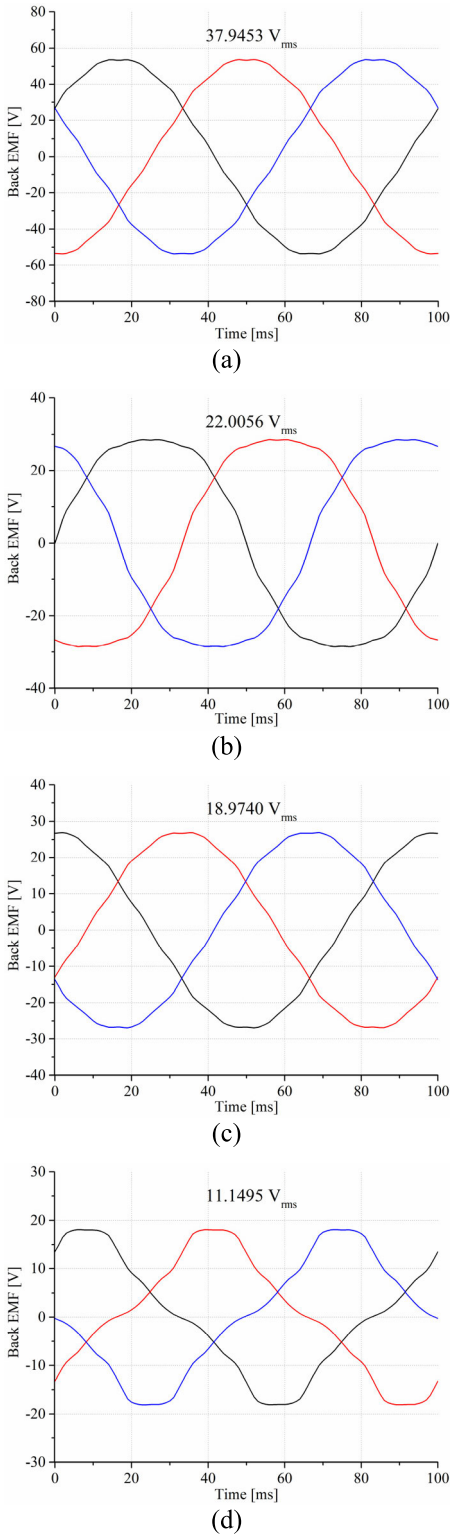

FIGURE 7. Simulated line back EMFs in (a) mode I; (b) mode II; (c) mode III; (d) mode IV.

and produces a negative torque component. It also introduces additional copper losses, and therefore, heat. Hence, the machine should have a low third-harmonic component of the back EMF to maintain adequate temperature and efficiency. Because we also increased line current for delta connections, the copper losses in power line also increased. However, these losses are typically negligible.

The machine transients during winding switching are shown in Figs. 9(a)–(c). During the simulations, all switches were toggled simultaneously, according to Table 1.

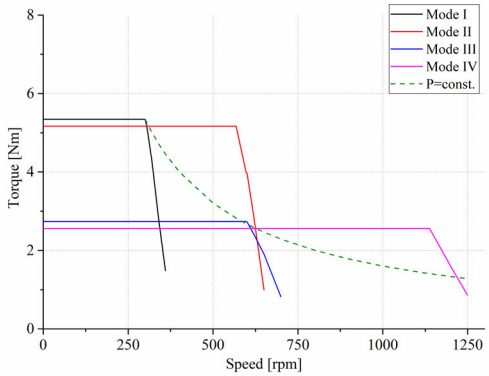

FIGURE 8. Torque-speed curves of the machine.

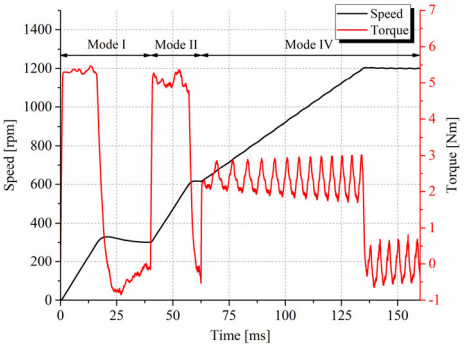

(a)

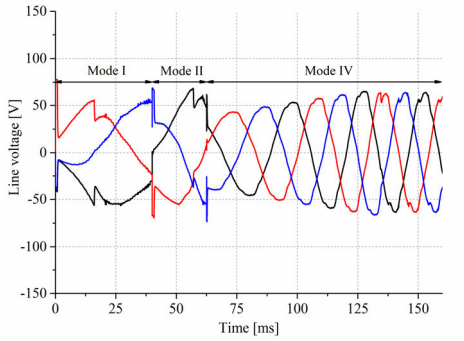

(b)

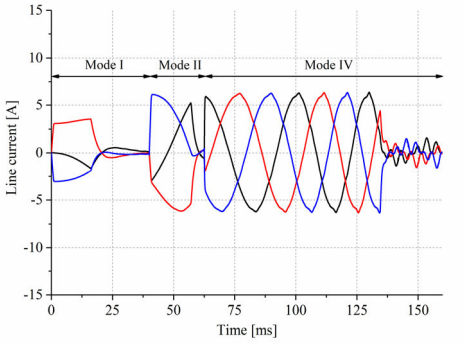

(c)

FIGURE 9. Simulated machine transients: (a) torque transients; (b) line voltage transients; (c) line current transients.

Initially, the machine was started in mode I, switches S1–S3 and S7–S9 were turned on, while S4–S6 and S10–S12 were turned off. The transition from mode I to mode II was performed at 300 rpm. For this transition, switches S7–S9 and S10–S12 were toggled at the same moment. Next, the transition from mode II to mode IV was performed at 600 rpm. In this case, switches S1–S3 and S4–S6 were toggled. The torque and speed transients are given in Fig. 9(a); as can be observed, the torque response was almost immediate. The line voltage and phase current transients are shown in Figs. 9(b) and (c), respectively. There was no abrupt current or voltage increase; hence, the winding could be safely switched during the machine run.

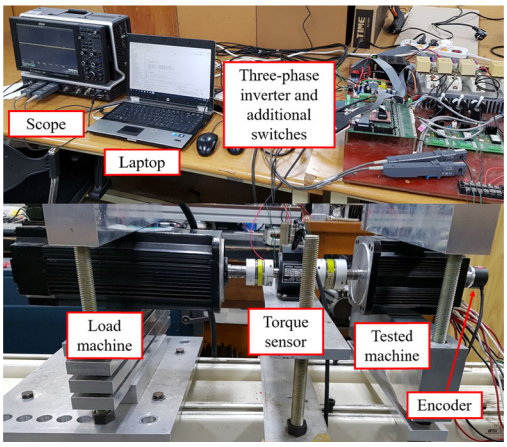

(a)

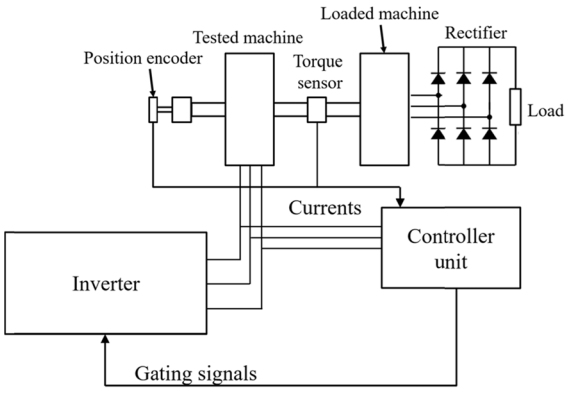

(b)

FIGURE 10. (a) Experimental setup. (b) Block diagram of the experimental setup.

V. EXPERIMENTAL VERIFICATION

To verify the possibility of CPO on a real prototype, the experimental setup, shown in Fig. 10(a) was arranged. The block diagram of this setup is shown in Fig. 10(b) for clarity. It consisted of a rewound three-phase SPM machine, three-phase bridge inverter, additional switches, a DSP controller, and scope. The low-power SPM machine parameters are listed in Table 3. Machine control was realized using RealSys control board with "Texas Instruments TMS320F28335" microcontroller. The TI TMS320F28335 is a real-time microcontroller with 150 MHz frequency, 68 KB RAM, 4 MB Flash

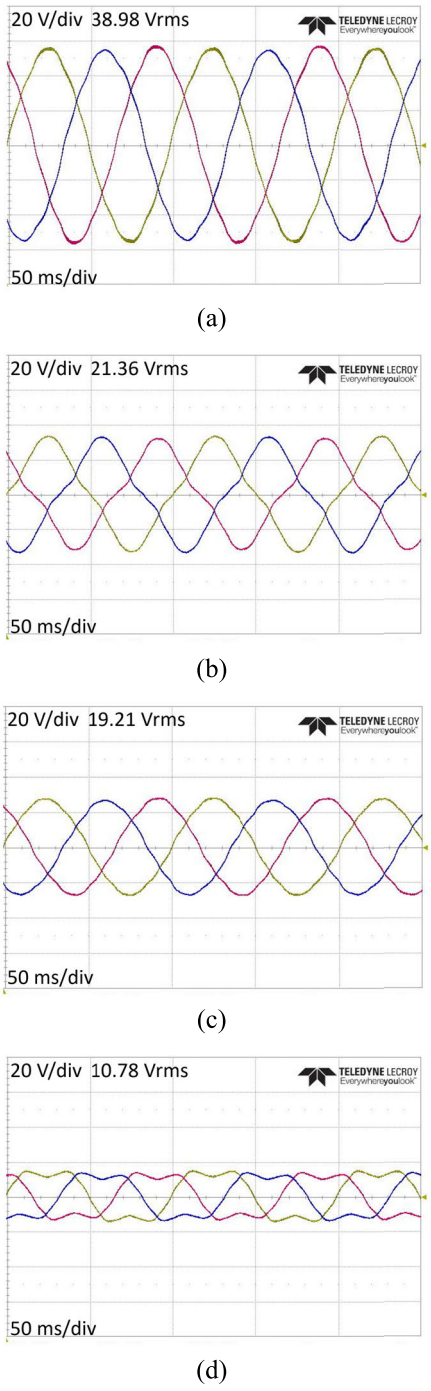

FIGURE 11. Measured back EMF in (a) mode I; (b) mode II; (c) mode III; (d) mode IV.

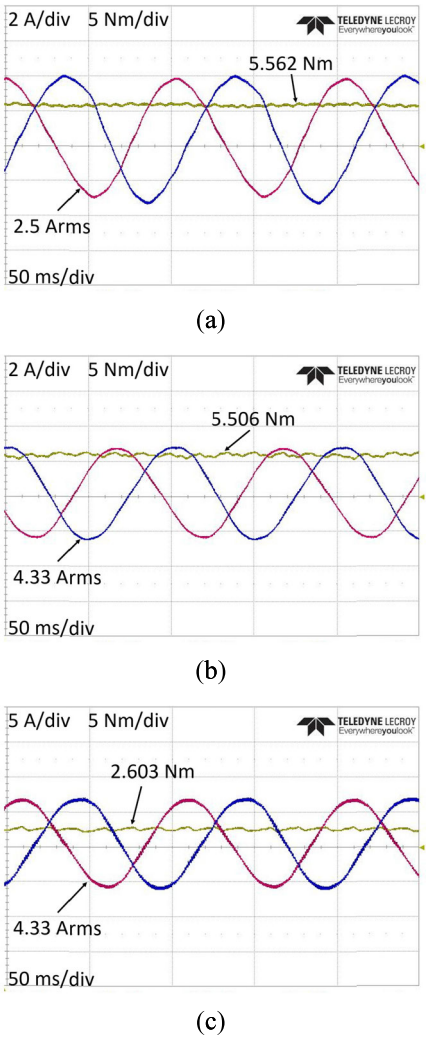

FIGURE 12. Measured torque and currents in (a) mode I; (b) mode II; (c) mode IV.

memory, 12 PWM channels, 4 ADC inputs, and 64 GPIO pins. It is supports I2C, McBSP, and SPI bus interfaces. Encoder E40S8 was used as a position sensor and connected with the control board through the ADC port. A three-phase bridge inverter was built using six "SEMIKRON SKM75GB128D" IGBTs, which were connected to the gating circuit. The gating circuit was controlled through the PWM channels. Output torque was registered by the torque sensor. Three hall current sensors were used to register stator currents. Additional bidirectional switches were realized using pairs of anti-series-connected IGBTs. Machine control was realized using a "Texas Instruments TMS320F28335" microcontroller and C-code compiler. The oscilloscope was a "LeCroy WaveRunner 604Zi" with differential voltage probes.

A. STEADY-STATE EXPERIMENTS

The line back EMF was measured at 300 rpm to verify that the flux linkage decreased. The tested machine shaft was coupled to the brushless DC (BLDC) motor rotating at a constant speed. The line back EMF was measured at open-ended terminals of the tested machine using three differential probes in each mode. As shown in Figs. 11(a)–(d), it was 38.65 V_{rms} in mode I, 22.43 V_{rms} in mode II, 19.28 V_{rms} in mode III, and 11.37 V_{rms} in mode IV. The K_2, K_3, and K_4 ratios can be found from the back EMFs because they are proportional to the rotational speed and flux linkage. The experimentally measured ratios were $K_2 = 1.72$, $K_3 = 2.00$, and $K_4 = 3.40$. These results agree well with the simulated results presented in Table 3.

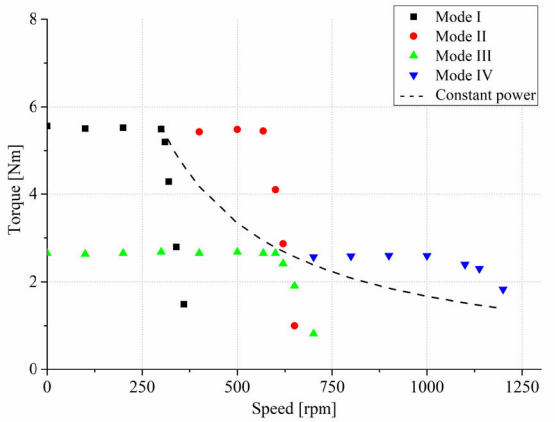

FIGURE 13. Measured torque-speed curves.

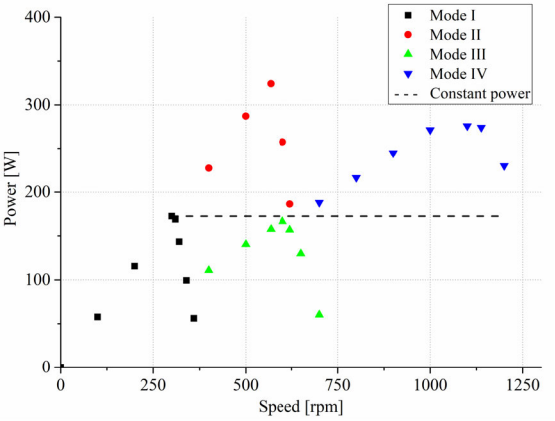

FIGURE 14. Measured power-speed curves of the machine.

The setup for loaded experiments is shown in Fig. 10(b). To perform the loaded experiments, the shaft of the tested machine was coupled to the BLDC using a torque sensor. The input terminals of the tested SPM machine were connected to the inverter, and the output of the BLDC was connected to the three-phase diode rectifier. The cascaded speed and current PID control were used. Current was controlled in the *dq0* reference frame. The output of the rectifier was connected to a resistive load. The SPWM modulator with a carrier frequency of 18 kHz generated gating signals for the inverter. As explained in subsection III. B, because mode III is redundant for the machine operation, the loaded experiment was performed for modes I, II, and IV. The steady-state torque at the rated speed and line currents are shown in Figs. 12(a)–(c), where blue and red lines represent line currents, and the yellow line represents torque. Average torques were 5.56 Nm, 5.506 Nm, 2.60 Nm, in modes I, II, and IV, respectively. Consequently, the power was 174.67 W, 172.97 W, and 81.68 W, respectively, in these modes.

A series of loaded experiments were performed at variable speeds. The torque-speed capability curves of the machine were plotted based on the measured results, as shown in Fig. 13. In this figure, the dashed line represents the torque for the CPO. The machine could exceed the rated power; thus, the CPO in the proposed method has the advantage of operation at a decreased phase current. The maximal speed at the rated output power was 1200 rpm, resulting in a CPSR of 4 pu. Based on these data, the power-speed curves were plotted, and are shown in Fig. 14. This figure also verifies CPO capability with the proposed winding layout.

TABLE 4. Comparison of the FEA and experimental results.

	FEA	Experimental results
Back EMF in modes I/II/III/IV [Vrms]	37.94/22.01/18.97/11.15	38.98/21.36/19.21/10.78
Torque in modes I/II/III/IV [Nm]	5.34/5.17/2.74/2.55	5.56/5.51/2.71/2.60
Maximum constant power speed [rpm]	1230	1210
Rated power [W]	167.88	174.67

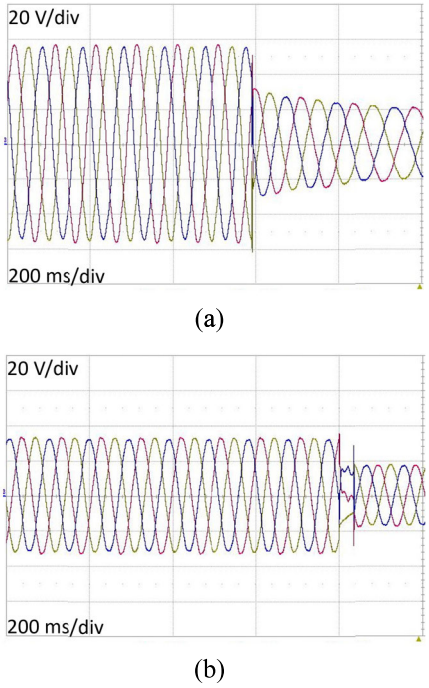

FIGURE 15. Measured back EMF transients during the winding switching. (a) From mode I to mode II; (b) from mode II to mode IV.

A comparison of the experimental results with the FEA results is presented in Table 4. The back EMF and torque values are listed for different modes and separated by a slash. It is clear that these results match well, with a deviation of not more than 6.17%. This deviation is caused by manufacturing imperfections.

B. TRANSIENT EXPERIMENTS

The additional current bi-directional switches were built using anti-series connected "SEMIKRON SKM75GB128D" IGBTs. The switching process was described in section IV. The back EMF transient tests during winding switching from Mode I to Mode II, and from Mode II to Mode IV are shown

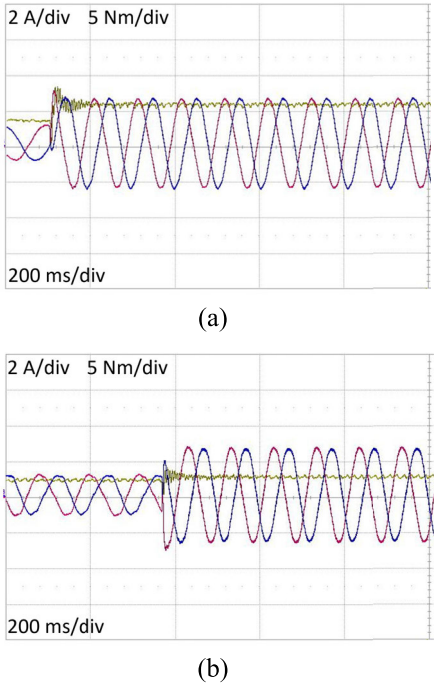

FIGURE 16. Measured torque transients and current transients during winding switching. (a) From mode I to mode II; (b) from mode II to mode IV.

in Figs. 15(a) and (b), respectively. There were no voltage spikes during the winding switching because the current in the phases was zero.

Figs. 16(a)–(b) show the current transients at the rated torque. As shown in Fig. 16(a), the transition from mode I to mode II was performed at a decreased line current because the resistive load was matched for mode II. The back EMF decreased after the winding switching; hence, the current rose to the rated RMS value. Consequently, the machine was accelerated until the voltage limit. A similar winding switching from mode II to IV is shown in Fig. 16(b). The resistive load was matched for mode IV; therefore, the current and torque increased after the transition, as shown in Fig. 16(a). It should be noted that no considerable current spikes were registered. This verifies the feasibility of the proposed winding switching method.

VI. CONCLUSION

In this study, a winding switching method was proposed for the extended CPSR of an SPM machine. In this study, it was shown that CPO using the proposed method can be achieved by choosing a suitable shift angle between ABC and XYZ sub-phase sets. The requirements for the CPO were formulated. For the given machine, the switching interconnection between the sub-phases allowed the production of different amounts of flux linkages in the machine phases, resulting in different rated speeds. In modes I, II, and IV, the rated speeds were 300, 568, and 1103 rpm, respectively. The presented experimental results demonstrated that the machine could maintain a rated power of 167.88 W until 1210 rpm; therefore, the CPSR was extended to 4 pu, compared to the basic three-phase machine. The dynamic experiment showed the possibility of winding switching during machine operation. These findings lay a foundation for the implementation of the proposed winding switching in constant power applications, such as traction and electric vehicles. The trade-off however, is the increased cost due to the additional switching circuit and rewinding.

REFERENCES

[1] S. Morimoto, Y. Takeda, and T. Hirasa, "Current phase control methods for permanent magnet synchronous motors," *IEEE Trans. Power Electron.*, vol. 5, no. 2, pp. 133–139, Apr. 1990, doi: 10.1109/63.53150.
[2] S. Morimoto, Y. Takeda, T. Hirasa, and K. Taniguchi, "Expansion of operating limits for permanent magnet motor by current vector control considering inverter capacity," *IEEE Trans. Ind. Appl.*, vol. 26, no. 5, pp. 866–871, Sep./Oct. 1990, doi: 10.1109/28.60058.
[3] R. F. Schiferl and T. A. Lipo, "Power capability of salient pole permanent magnet synchronous motors in variable speed drive applications," *IEEE Trans. Ind. Appl.*, vol. 26, no. 1, pp. 115–123, Jan./Feb. 1990, doi: 10.1109/28.52682.
[4] K. Atallah, D. Howe, P. H. Mellor, and D. A. Stone, "Rotor loss in permanent magnet brushless AC machines," in *Proc. IEEE Int. Electr. Mach. Drives Conf. (IEMDC)*, Seattle, WA, USA, May 1999, pp. 60–62, doi: 10.1109/IEMDC.1999.769027.
[5] S. Chaithongsuk, B. Nahid-Mobarakeh, J.-P. Caron, N. Takorabet, and F. Meibody-Tabar, "Optimal design of permanent magnet motors to improve field-weakening performances in variable speed drives," *IEEE Trans. Ind. Electron.*, vol. 59, no. 6, pp. 2484–2494, Jun. 2012, doi: 10.1109/TIE.2011.2164770.
[6] T. Sebastiangordon and G. R. Slemon, "Operating limits of inverter-driven permanent magnet motor drives," *IEEE Trans. Ind. Appl.*, vol. IA-23, no. 2, pp. 327–333, Mar. 1987, doi: 10.1109/TIA.1987.4504909.
[7] O. Ustun, O. C. Kivanc, S. Senol, and B. Fincan, "On field weakening performance of a brushless direct current motor with higher winding inductance: Why does design matter?" *Energies*, vol. 11, no. 11, pp. 3119–3135, Nov. 2018.
[8] S.-M. Sue, J.-H. Liaw, Y.-S. Huang, and Y.-H. Liao, "Design and implementation of a dynamic voltage boosting drive for permanent magnet synchronous motors," in *Proc. Int. Power Electron. Conf. (ECCE, ASIA)*, Sapporo, Japan, Jun. 2010, pp. 1398–1402, doi: 10.1109/IPEC.2010.5544573.
[9] J. Zhang, J.-S. Lai, R.-Y. Kim, and W. Yu, "High-power density design of a soft-switching high-power bidirectional DC–DC converter," *IEEE Trans. Power Electron.*, vol. 22, no. 4, pp. 1145–1153, Jul. 2007.
[10] E. Nipp, "Permanent magnet motor drives with switched stator windings," Ph.D. dissertation, Roy. Inst. Technol., Stockholm, Sweden, 1999.
[11] H. Huang and L. Chang, "Electrical two-speed propulsion by motor winding switching and its control strategies for electric vehicles," *IEEE Trans. Veh. Technol.*, vol. 48, no. 2, pp. 607–618, Mar. 1999.
[12] M. Wang, N. Hsu, C. Chiang, S. Wang, and T. Shau, "A novel changeover technique for variable-winding brushless DC motor drives," in *Proc. SICE Annu. Conf.*, Taipei, Taiwan, 2010, pp. 2650–2653.
[13] H. Hijikata, Y. Sakai, K. Akatsu, Y. Miyama, H. Arita, and A. Daikoku, "Wide speed range operation by low-voltage inverter-fed MATRIX motor for automobile traction motor," *IEEE Trans. Power Electron.*, vol. 33, no. 8, pp. 6887–6896, Aug. 2018.
[14] M. M. Swamy, T. Kume, A. Maemura, and S. Morimoto, "Extended high-speed operation via electronic winding-change method for AC motors," *IEEE Trans. Ind. Appl.*, vol. 42, no. 3, pp. 742–752, May/Jun. 2006, doi: 10.1109/TIA.2006.873657.
[15] F. Copt, D. M. Araujo, C. Koechli, and Y. Perriard, "Current control strategy for dynamic winding reconfiguration of slotless brushless DC motors," *IEEE Trans. Ind. Appl.*, vol. 55, no. 1, pp. 417–425, Jan./Feb. 2019, doi: 10.1109/TIA.2018.2869102.
[16] S.-H. Im and B.-G. Gu, "A snubberless solid-state tap changer for permanent magnet synchronous motors," *IEEE Trans. Power Electron.*, vol. 35, no. 11, pp. 12143–12152, Nov. 2020, doi: 10.1109/TPEL.2020.2988933.
[17] S. Hemmati and T. A. Lipo, "Field weakening of a surface mounted permanent magnet motor by winding switching," in *Proc. Int. Symp. Power Electron. Power Electron., Electr. Drives, Automat. Motion*, Sorrento, Italy, 2012, pp. 736–740, doi: 10.1109/SPEEDAM.2012.6264472.

[18] S. Atiq, T. A. Lipo, and B.-I. Kwon, "Wide speed range operation of non-salient PM machines," *IEEE Trans. Energy Convers.*, vol. 31, no. 3, pp. 1179–1191, Sep. 2016, doi: 10.1109/TEC.2016.2547421.
[19] S. Atiq, T. A. Lipo, and B. Kwon, "Experimental verification of winding switching technique to enhance maximum speed operation of surface mounted permanent magnet machines," *IET Electr. Power Appl.*, vol. 10, no. 4, pp. 294–303, Apr. 2016, doi: 10.1049/iet-epa.2015.0274.
[20] S. Atiq and B.-I. Kwon, "Susceptibility of the winding switching technique for flux weakening to harmonics and the choice of a suitable drive topology," *Int. J. Electr. Power Energy Syst.*, vol. 85, pp. 22–31, Feb. 2017.
[21] A. Arif, N. Baloch, and B.-I. Kwon, "Winding switching and turn switching in permanent magnet Vernier machines for wide speed range operation and high efficiency," *IEEE Access*, vol. 7, pp. 55344–55357, 2019, doi: 10.1109/ACCESS.2019.2912181.
[22] S. Sin, M. Ayub, and B.-I. Kwon, "Operation method of non-salient permanent magnet synchronous machine for extended speed range," *IEEE Access*, vol. 8, pp. 105922–105935, 2020, doi: 10.1109/ACCESS.2020.3000256.
[23] S. Sin, M. Ayub, and B.-I. Kwon, "Investigation study of multi-mode multi-speed operation method for surface-mounted permanent magnet synchronous machines," *IEEE Access*, vol. 8, pp. 169470–169485, 2020, doi: 10.1109/ACCESS.2020.3024183.

STANISLAV SIN was born in 1994. He received the B.S. degree in electronics engineering from the Ferghana Polytechnic Institute, Ferghana, Uzbekistan, in 2016. He is currently pursuing the M.S. degree with the Department of Electrical and Electronic Engineering, Hanyang University, Ansan, South Korea. His research interests include electric machine control and power electronics.

ALI ROSHANZAMIR was born in 1986. He received the B.S. degree in control engineering from Applied Science University, Iran, in 2012. He is currently pursuing the Ph.D. degree with the Department of Electrical and Electronic Engineering, Hanyang University, Ansan, South Korea. From 2011 to 2016, he was a Co-Researcher with the Control and Robotic Laboratory, Institute of Advance Science and Technology, IRAN SSP Research and Development Center. His research interests include nonlinear control, magnetic bearing design, electric machine design, and control.

BYUNG-IL KWON (Senior Member, IEEE) was born in 1956. He received the B.S. and M.S. degrees in electrical engineering from Hanyang University, Ansan, South Korea, in 1981 and 1983, respectively, and the Ph.D. degree in electrical engineering and machine analysis from the University of Tokyo, Tokyo, Japan, in 1989. From 1989 to 2000, he was a Visiting Researcher with the Faculty of Science and Engineering Laboratory, University of Waseda, Tokyo. In 1990, he was a Researcher with the Toshiba System Laboratory, Yokohama, Japan. In 1991, he was a Senior Researcher with the Institute of Machinery and Materials Magnetic Train Business, Daejeon, South Korea. From 2001 to 2008, he was a Visiting Professor with the University of Wisconsin–Madison, Madison, WI, USA. He is currently a Professor with Hanyang University. His research interests include design and control of electric machines.